NUMERICAL SIMULATION OF FLOW DATA OVER TWO-DIMENSIONAL HILLS

R. YING*, V. M. CANUTO and R. M. YPMA
NASA, Goddard Institute for Space Studies, New York, N.Y., 10025, U.S.A

(Received in final form 1 March, 1994)

Abstract. We have studied a neutrally-stratified flow over two-dimensional hills using a two-dimensional, non-hydrostatic version of the Regional Atmospheric Modeling System (RAMS). We have implemented three different turbulence closure models: the standard $E-\epsilon$ model, an Algebraic Reynolds Stress Model (ARSM) and a new $E-\epsilon-\overline{uw}$ model. Model predictions for the mean and turbulence flows using different closure schemes are compared with the data of a wind tunnel experiment containing isolated two-dimensional hills of varying slope. From the comparison, it is concluded that all three models predict the mean flow velocities equally well while only the new $E-\epsilon-\overline{uw}$ closure model accurately predicts the turbulence data statistics.

1. Introduction

The determination of the turbulent wind field over complex terrain in the Atmospheric Boundary Layer (ABL) has been a topic of numerous past studies. Due to the mathematical difficulties involved in modelling the flow structure, the mean flow either has been assumed to be a simplified type of flow (e.g., potential flow) or has been obtained by solving linearized equations of motion with crude assumptions about turbulence. Inevitably, the underlying assumptions of these models limited their applicability to gentle relief. Indeed, these models fail to reproduce certain important features of the complicated flow structure over complex terrain, especially when the terrain slope is moderate or steep. Consequently, it is now recognized that in order to understand how irregularities of the ground surface distort the mean and turbulent structure of the incident flow, and thus obtain a complete picture of the flow structure, it is necessary to solve a full set of fluid dynamics equations using finite-difference or more sophisticated numerical methods.

It has been shown in many studies that in steady-state, neutrally-stratified ABL flow over topography, the mean velocity changes are relatively insensitive to the turbulence closure scheme (see Hunt and Simpson, 1982; Taylor *et al.*, 1987). On the other hand, the characteristics of the turbulence depend very sensitively on the closure scheme adopted (Taylor *et al.*, 1987). Simple schemes, such as the mixing-length model, which are essentially local in nature, are adequate only if there is a near equilibrium between local production and dissipation rates of turbulent kinetic energy. Because of the extreme sensitivity of the turbulent field to the varying pressure gradients caused by the terrain, these models are not

* The research reported in this paper was conducted while the first author held a National Research Council (NRC) Associateship.

Boundary-Layer Meteorology **70:** 401–427, 1994.

applicable to the case of complex terrain. In fact, observations of turbulence structure over hills are poorly reproduced by mixing-length models (Bradley, 1980; Britter *et al.*, 1981; Mason and King, 1985). In general, for complex terrain, non-equilibrium effects become significant, and thus a realistic description of the turbulence structure requires considerably more sophisticated closures (Zeman and Jensen, 1987).

Several years of experimental and theoretical work have helped to elucidate some basic features of the turbulence dynamics concerning neutrally-stratified boundary-layer flow over a hill. In brief, there are two fundamental time scales: the first is the "time of flight" t_d, which is the travel time for an eddy starting upstream to be advected along a streamline; the second is the turbulence time scale t_l, which is the time taken for an eddy to decorrelate or turnover. The changes in the structure of turbulence over a hill depend on the relative magnitude of these two scales. In the outer region, defined by $t_d \leq t_l$, the already complex upstream boundary-layer turbulence is subject to rapid distortion. In rapid distortion theory, it is assumed that the turbulent eddies are distorted by the mean flow so rapidly that the turbulence is not significantly modified by the change of strain rate (i.e., by the production terms). Consequently, in the outer region, the change in turbulence depends on the history of the mean flow and not on the local velocity gradient. In a thin, inner region adjacent to the surface, defined by $t_d \geq t_l$, the eddy-eddy interactions are more important than the straining by the distorted mean flow, and thus the flow can be expected to be in local equilibrium with the surface. In the intermediate region, where $t_d \sim t_l$, it is clear that the changes in the turbulence are diverse and a high-order turbulence closure model is needed to allow a match between the inner and outer regions.

It is known that the occurrence of flow separation in the lee of hills sometimes gives rise to a reversed flow and high turbulence intensities (Taylor *et al.*, 1987). Turbulence modeling in the atmosphere has rarely included cases of abrupt topography where flow separation occurs. Computations of atmospheric flows have generally focused on large-scale phenomena in which recirculation zones were either absent or much smaller than the grid scale used in the calculation.

In addition, most atmospheric models are based on the hydrostatic approximation. They cannot numerically treat recirculating flows because the acceleration of the vertical velocity is neglected. In this regard, atmospheric turbulence modeling has lagged behind engineering turbulence modeling. In engineering applications (Rodi, 1984), the $K-\epsilon$ model ($E-\epsilon$ in the meteorology literature) has predicted recirculating flows with an accuracy acceptable for most purposes. Rodi concluded that the mixing-length hypothesis is not suitable for recirculating flows, and there is little evidence to support the belief that the length scale specifications used in one-equation models (where only the transport equation for turbulent kinetic energy is solved) are sufficiently universal for these flows. As to higher-

order turbulence closure models, there have been too few applications to allow an assessment of their performance in predicting recirculating flows.

Concerning flow and turbulence in the ABL, two types of experiments exist, i.e., field experiments and wind tunnel experiments. Field experiments provide real-world data and, in this sense, are more reliable. However, generalization of field data is difficult because of the peculiarities of specific sites and meteorological conditions. Controlled variation of independent variables is also generally impossible. In contrast to field experiments, wind tunnel experiments can simulate the flow field in the ABL with the possibility of controlling the governing parameters and reproducing the experimental conditions. In the past, though many wind tunnel experiments were performed, they had relatively little influence on the development of the theory mostly due to the difficulty of obtaining reliable measurements in the region very close to the surface. The lack of reliance on wind tunnel data is unfortunate because, provided that the limitations of wind tunnel modeling are properly accounted for, one can make good use of the valuable information contained in the data.

Considering the many advantages of wind tunnel experiments over field experiments, we shall compare our theoretical models to the wind tunnel data with hills of idealized shape. In this way, we hope to obtain a basic understanding of the physical processes involved as well as of the principal governing parameters. Specifically, we adopt the EPA wind tunnel experiment RUSHIL (Khurshudyan *et al.*, 1981), which provides complete mean and turbulent field data for a neutrally-stratified flow over isolated, two-dimensional hills of variable slope.

In this study, we solve a full set of primitive non-hydrostatic dynamic equations for mean flow quantities using a finite-difference method. The numerical code RAMS (the Regional Atmospheric Modeling System of Colorado State University) will be employed to perform the numerical calculations. To account for the complex terrain, we use the terrain-following coordinate system available in RAMS (Clark, 1977), in which an irregular lower boundary is transformed into a plane.

From past experience, it seems that in hilly cases like the ones we study, a two-equation turbulence closure model would be the simplest model that promises success. Based on this consideration, we have implemented in RAMS the following turbulence models: (1) a standard $E - \epsilon$ model which consists of prognostic equations for the turbulent kinetic energy E and the energy dissipation rate ϵ; (2) an Algebraic Reynolds Stress Model (ARSM), which determines the Reynolds stresses through algebraic equations; (3) an $E - \epsilon - \overline{uw}$ model, which has three prognostic equations for E, ϵ, and the vertical momentum flux $\overline{uw}$. The performance of these different closures is evaluated through comparison of model results with wind tunnel data.

2. Description of the Model

2.1. Non-hydrostatic flow model over complex terrain

A full set of primitive non-hydrostatic dynamic equations is solved in this study. Derivations of the momentum and pressure equations require the use of an equation of state and the continuity equation. The equation of state for dry air is

$$\Pi = \left(\frac{R}{p_{00}}\rho\Theta\right)^{R/c_v}, \tag{1}$$

where Π is the Exner function, R is the gas constant for dry air, p_{00} is the base state pressure at the ground, ρ is the density of dry air, Θ is the potential temperature, and c_v is the specific heat at constant volume.

The compressible continuity equation is

$$\frac{\partial\rho}{\partial t} + \frac{\partial}{\partial x_j}(\rho U_j) = 0, \tag{2}$$

where U_j is the velocity component in *the* x_j direction.

The momentum equations, derived from the Navier–Stokes equations with the aid of Equation (1), are

$$\frac{\mathrm{d}\overline{U_i}}{\mathrm{d}t} + c_p\Theta_0\frac{\partial\pi'}{\partial x_i} = \delta_{i3}g\left(\frac{\overline{\Theta}}{\Theta_0} - 1\right) - \frac{\partial}{\partial x_j}\overline{u_i u_j}, \tag{3}$$

where $\mathrm{d}/\mathrm{d}t = \partial/\partial t + \overline{U}_j\partial/\partial x_j$ is the substantial derivative, c_p is the specific heat at constant pressure, $\overline{U}_i$ and $\overline{\Theta}$ are the ensemble means of U_i and Θ, π' is the deviation of Π from the initial unperturbed state Π_0, and $\overline{u_i u_j}$ are the Reynolds stresses. The initial unperturbed state (represented by the pressure Π_0, potential temperature Θ_0 and density ρ_0) is the atmosphere at rest, where the hydrostatic equilibrium is assumed, i.e., $\partial\Pi_0/\partial z = -g/(c_p\Theta_0)$.

The pressure equation is derived by taking the substantial derivative of Equation (1) and using Equation (2)

$$\frac{\partial\pi'}{\partial t} + \frac{R\Pi_0}{c_v\rho_0\Theta_0}\frac{\partial}{\partial x_j}(\rho_0\Theta_0\overline{U_j}) = f_\pi. \tag{4}$$

The terms contained in f_π have little influence on the processes of physical interest (Klemp and Wilhelmson, 1978), and are therefore put equal to zero in our calculation.

Finally, the equation for the potential temperature is

$$\frac{\mathrm{d}\overline{\Theta}}{\mathrm{d}t} = -\frac{\partial}{\partial x_j}\overline{u_j\theta}, \tag{5}$$

where $\overline{u_j\theta}$ are the turbulent heat fluxes.

The salient feature of the above basic equations is the incorporation of a non-hydrostatic pressure Equation (4). In many atmospheric models, the pressure is calculated from a hydrostatic equation. The latter is valid only when the horizontal length scale of the phenomenon modeled is greater than the density-scaled height of the atmosphere. Under this condition, the vertical acceleration can be neglected and the vertical momentum equation reduces to the hydrostatic equation (Pielke, 1984). In hill cases like the ones treated here, however, the varying pressure gradient causes horizontal structures whose scales are smaller than the density-scaled height. The hydrostatic assumption is no longer valid and thus a non-hydrostatic equation for the pressure calculation is required. Indeed, the vertical velocity field resulting from our numerical calculation clearly shows that the vertical acceleration cannot be neglected.

In the presence of complex terrain with surface height $z_g(x, y)$ and height of the computational domain s, Equations (3)–(5) are transformed into the terrain-following coordinate system (x, y, η), which is related to the Cartesian coordinates (x, y, z) by (Clark, 1977)

$$\eta = s\frac{z - z_g(x, y)}{s - z_g(x, y)}. \tag{6}$$

Specification of the function $z_g(x, y)$ will be made in 5.2 below.

2.2. The Turbulence Closure Schemes

2.2.1. The Standard $E - \epsilon$ Model

In this scheme, the Reynolds stresses in Equation (3) and the heat fluxes in Equation (5) are computed from the eddy viscosity assumption:

$$\overline{u_i u_j} = -\nu_t\left(\frac{\partial\overline{U_i}}{\partial x_j} + \frac{\partial\overline{U_j}}{\partial x_i}\right) + \frac{2}{3}\delta_{ij}E, \tag{7}$$

$$\overline{u_i\theta} = -\frac{\nu_t}{\sigma_t}\frac{\partial\overline{\Theta}}{\partial x_i}, \tag{8}$$

where ν_t is the eddy viscosity and σ_t is the turbulent Prandtl number. Here, ν_t is supposed to be proportional to the turbulent velocity and length scales. In the hilly cases, due to the non-equilibrium effects and other complexities caused by the hill, ν_t can not be specified in a simple manner such as in the mixing-length theory, $\nu_t \propto \hat{v}l_m$, where $\hat{v}$ and l_m are a rms turbulent velocity and a mixing length. In a two-equation model, the turbulent kinetic energy E, characterizing the turbulent velocity scale, and a quantity related to the turbulent length scale are solved by transport equations. These equations account for advection, diffusion, production and dissipation of the turbulent velocity scale and length scale. Among different types of two-equation models that have been discussed in the literature,

namely, $E-\epsilon$, $E-\tau$, $E-\omega$ and $E^{1/2}-\omega$, where $\tau = 2E/\epsilon$ and $\omega = \epsilon/E$ (since $\epsilon \sim E^{3/2}/l$, where l is the dissipation length scale, all of these quantities are related to l), Lang and Shih (1991) have concluded that the $E-\epsilon$ model is the most robust in the sense that it requires the least number of changes when considering different types of flows. The $E-\epsilon$ model is not only very popular and successful in engineering studies, but it has also been applied to atmospheric flows with considerable success (Detering and Etling, 1985; Beljaars *et al.*, 1987; Duynkerke, 1988).

In the $E-\epsilon$ model, ν_t is given by

$$\nu_t = c_\mu \frac{E^2}{\epsilon}, \tag{9}$$

where c_μ is a constant.

The transport equations for the turbulent kinetic energy E and dissipation rate ϵ are

$$\frac{\mathrm{d}E}{\mathrm{d}t} = \frac{\partial}{\partial x_j}\left(\frac{\nu_t}{\sigma_e}\frac{\partial E}{\partial x_j}\right) + P - \epsilon, \tag{10}$$

$$\frac{\mathrm{d}\epsilon}{\mathrm{d}t} = \frac{\partial}{\partial x_j}\left(\frac{\nu_t}{\sigma_\epsilon}\frac{\partial \epsilon}{\partial x_j}\right) + \frac{\epsilon}{E}(c_{1\epsilon}P - c_{2\epsilon}\epsilon), \tag{11}$$

where σ_e, σ_ϵ, $c_{1\epsilon}$ and $c_{2\epsilon}$ are constants, and P is the rate of production of turbulent kinetic energy given by

$$P = -\overline{u_i u_j}\frac{\partial \overline{U_i}}{\partial x_j}. \tag{12}$$

In the above equations, the values of the constants ($c_\mu = 0.09$, $c_{1\epsilon} = 1.44$, $c_{2\epsilon} = 1.92$, $\sigma_e = 1$, $\sigma_\epsilon = 1.13, \sigma_t = 0.9$) are taken from Launder and Spalding (1974).

2.2.2. *The Algebraic Reynolds Stress Model*

In order to allow for the different evolution of the various turbulent stresses (representing various velocity scales in complex flows) and to properly account for their transport, models were developed which employ transport equations for the individual Reynolds stresses $\overline{u_i u_j}$. After modeling the pressure-correlation and dissipation terms according to Rodi (1984), the transport equation for $\overline{u_i u_j}$ is written as

$$\begin{aligned}\frac{\mathrm{d}\overline{u_i u_j}}{\mathrm{d}t} &= \mathrm{Diff}(\overline{u_i u_j}) + P_{ij} - c_1\frac{\epsilon}{E}\left(\overline{u_i u_j} - \frac{2}{3}\delta_{ij}E\right) \\ &\quad -\gamma\left(P_{ij} - \frac{2}{3}\delta_{ij}P\right) - \frac{2}{3}\epsilon\delta_{ij}.\end{aligned} \tag{13}$$

On the right hand side of (13), the first term is the diffusion term, the second term $P_{ij} = -(\overline{u_i u_l}\partial\overline{U_j}/\partial x_l + \overline{u_j u_l}\partial\overline{U_i}/\partial x_l)$ is the production term, the third and the fourth terms with constant coefficients c_1 and γ are modeled pressure-correlation terms, and the last term represents dissipation.

A simplified form of the transport equations for $\overline{u_i u_j}$ is the Algebraic Reynolds Stress Model (ARSM) proposed by Rodi (1984). In this model, the sum of the transport terms of $\overline{u_i u_j}$ in Equation (13), including the rate of change, advection and diffusion terms, is assumed to be proportional to that of E, the proportionality factor being the ratio $\overline{u_i u_j}/E$ (which is not a constant). One writes

$$\frac{\mathrm{d}\overline{u_i u_j}}{\mathrm{d}t} - \mathrm{Diff}(\overline{u_i u_j}) = \frac{\overline{u_i u_j}}{E}\left[\frac{\mathrm{d}E}{\mathrm{d}t} - \mathrm{Diff}(E)\right], \tag{14}$$

which on the basis of Equation (10) becomes

$$\frac{\mathrm{d}\overline{u_i u_j}}{\mathrm{d}t} - \mathrm{Diff}(\overline{u_i u_j}) = \frac{\overline{u_i u_j}}{E}(P - \epsilon). \tag{15}$$

Substituting Equation (15) into Equation (13) gives the ARSM

$$\overline{u_i u_j} = E\left[\frac{2}{3}\delta_{ij} + \frac{(1-\gamma)\left(\frac{P_{ij}}{\epsilon} - \frac{2}{3}\delta_{ij}\frac{P}{\epsilon}\right)}{c_1 + \frac{P}{\epsilon} - 1}\right]. \tag{16}$$

In two-dimensional boundary-layer flows, calling $\overline{U}$ and u the components of the mean and turbulent velocities in the horizontal flow direction x, and $\overline{W}$ and w those in the vertical direction z, the shear stress $\overline{uw}$ is usually the one that exerts significant direct influence on the development of the mean flow. In this case, if the further approximation $\overline{u^2} = \overline{w^2} = (2/3)E$ is used in the P_{ij} term of Equation (16), one obtains an explicit expression for $\overline{uw}$,

$$\overline{uw} = -\frac{c_1'}{1 + \gamma'\frac{P}{\epsilon}}\frac{E^2}{\epsilon}\left(\frac{\partial\overline{U}}{\partial z} + \frac{\partial\overline{W}}{\partial x}\right), \tag{17}$$

where c_1' and γ' are positive constants. Equation (17) turns out to be an eddy viscosity relationship with the eddy viscosity given by

$$\nu_t = \frac{c_1'}{1 + \gamma'\frac{P}{\epsilon}}\frac{E^2}{\epsilon}, \tag{18}$$

which shows that ν_t is now a dynamical variable since it depends on the ratio P/ϵ.

2.2.3. The $E - \epsilon - \overline{uw}$ Model

As mentioned before, in two-dimensional boundary-layer flows, the shear stress $\overline{uw}$ is the most influential component of the Reynolds stress tensor. Thus, in this scheme, out of the full set of transport equations for the Reynolds stresses, only those for E, ϵ and $\overline{uw}$ are solved. The equations for E and ϵ are the same as in the standard $E - \epsilon$ model, while the equation for $\overline{uw}$ is

$$\frac{\mathrm{d}\overline{uw}}{\mathrm{d}t} = \frac{\partial}{\partial z}\left(\alpha^2 \frac{E^2}{\epsilon}\frac{\partial \overline{uw}}{\partial z}\right) + C_\phi\left[\frac{\epsilon}{E}\overline{uw} + \alpha^2 E\left(\frac{\partial \overline{U}}{\partial z} + \frac{\partial \overline{W}}{\partial x}\right)\right], \tag{19}$$

which is similar to the one derived by Hanjalic and Launder (1972).

The remaining Reynolds stress components are still computed from Equation (7) as in the standard $E - \epsilon$ model.

3. The EPA Wind Tunnel Experiment RUSHIL

The EPA wind tunnel experiment RUSHIL simulates a neutral atmospheric boundary layer with two-dimensional relief. The incoming flow (in the x direction) is characterized by a logarithmic velocity profile

$$\overline{U}(z) = \frac{u_*}{\kappa}\ln\left(\frac{z}{z_0}\right), \tag{20}$$

with $z_0 = 0.157 \times 10^{-3}$ m, $u_* = 0.178$ m/s, and $\kappa = 0.4$. This velocity profile reaches the free-stream velocity $U_\infty = 3.9$ m/s at the height of 1 m. A two-dimensional model hill of analytical shape is placed across the incoming flow, spanning the width of the tunnel (in the y direction). Three different model hills with a maximum height $h = 0.117$ m and different slopes were used. Their aspect ratios a/h (ratio of the half-width a to the height) were 8, 5 and 3, corresponding to maximum slope angles of 10°, 16° and 26°, respectively. These aspect ratios will be used as hill identifiers: Hill 8, Hill 5 and Hill 3.

Measurements of mean and turbulent velocity fields were taken upwind, over and downwind of each of the hills. Vertical profiles of the mean horizontal velocity $\overline{U}(z)$, the angle of mean velocity to horizontal surface $\Phi(z)$, the longitudinal and vertical turbulent intensities $\sigma_u(z)$ and $\sigma_w(z)$, and the Reynolds shear stress $\overline{uw}$ were measured at 16 longitudinal locations from $x/a = -2$ to $x/a \geq 5$, where $x = 0$ corresponds to the top of the hill. For reference purposes, all the measurements were also taken over the flat wind tunnel floor.

The EPA wind tunnel data, as originally reported, show a high degree of scatter, making them unsuitable for practical use. Recently, however, this serious drawback has been overcome by a group of meteorologists (Trombetti *et al.*, 1991). They realized that the experimental data sets require proper analysis in order to minimize measurement errors and produce fields consistent with certain

dynamic requirements. Consequently, they have undertaken the task of smoothing the EPA data. Each vertical profile of the flow data has been smoothed by taking into account the errors of experimental measurements and forced to the appropriate surface values; then each profile has been interpolated at regularly spaced levels and presented graphically.

4. Boundary Conditions and Initialization

Because the ground surface is impermeable, the mean flow at the lowest level follows the surface contour. At the lower boundary, the similarity law for a constant-stress surface layer is assumed. For $\overline{U}$, E and ϵ, the lower boundary conditions are applied at some height z_p within the surface layer

$$\overline{U}(z_p) = \frac{u_*}{\kappa} \ln\left(\frac{z_p}{z_0}\right), \tag{21}$$

$$E(z_p) = \frac{u_*^2}{c_\mu^{1/2}}, \tag{22}$$

$$\epsilon(z_p) = \frac{u_*^3}{\kappa z_p}, \tag{23}$$

where z_p is chosen as the half-grid level above the ground, u_* is the friction velocity and z_0 the roughness length. The boundary conditions for E and ϵ result from assuming that dissipation near the ground is balanced by the generation of turbulent kinetic energy. While this assumption may not agree well with the actual condition, it has been used extensively in other studies (Rodi, 1984), and is used here in the absence of better boundary conditions. For $\overline{uw}$, the lower boundary condition is applied at $z = 0$ in the form

$$\overline{uw}(z = 0) = u_*^2. \tag{24}$$

Our simulation domain is set to 2 m height, which is far removed from the region affected by the hilly terrain (which is about 1 m in height). Thus, the influence of the upper boundary is minimized. A rigid lid is assumed at the upper boundary, where the vertical velocity is set to zero and the pressure is adjusted to account for the perturbation caused by the underlying terrain at that level and to compensate for the restrictive requirement on vertical velocity (Klemp and Wilhelmson, 1978; Pielke, 1984).

The lateral boundaries are also located far from the hill region in order to minimize the influence of the boundaries. At the inflow boundary, variables are kept constant in time as

$$\overline{U}(z) = \overline{U}_0(z), \tag{25}$$

$$E(z) = E_0(z), \tag{26}$$

$$\epsilon(z) = \epsilon_0(z), \tag{27}$$

$$\overline{uw}(z) = \overline{uw_0}(z), \tag{28}$$

where $\overline{U}_0(z)$, $E_0(z)$, $\epsilon_0(z)$ and $\overline{uw_0}(z)$ are the output profiles from the simulations carried out in flat terrain. While running the simulations in flat terrain, the simulation domain was set sufficiently large in the flow direction in order for the flow to develop and finally reach equilibrium. The equilibrium, x-independent solutions are then used as input for the simulations in hilly terrain. At the outflow boundary, the gradient of $\overline{U}$ normal to the boundary is set equal to zero and the second-derivatives of the other variables in the direction normal to the boundary are also set equal to zero.

All the prognostic variables are initialized horizontally homogeneously with the same profiles as used for the inflow lateral boundary conditions in Equations (25)–(28).

5. Numerical Method

5.1. The computational grid

The model variables are defined on an Arakawa C staggered grid. In a two-dimensional case, the grid structure is shown in Figure 1. The vertical velocity $\overline{W}$ and the shear stress $\overline{uw}$ are staggered at half-grid points in the vertical with respect to the other dependent variables. The horizontal velocity $\overline{U}$ is staggered at half-grid points in the horizontal.

To obtain high vertical resolution near the ground and low resolution at higher levels, our model has the smallest grid increment near the ground, with the grid mesh expanding upward. In this vertically stretched grid, a constant expansion ratio is kept between consecutive levels, which is equivalent to a logarithmic scaling commonly used in the ABL modeling. The expansion ratio, however, is set to a small value of 1.1 because large ratios would destroy the second-order accuracy of the vertical differencing in the model. In this way, the vertical grid size is set to 0.005 m at the lowest level and stretched to 0.1 m at the level of 1 m; above 1 m, the grid size remains constant as 0.1 m.

An additional consideration in our simulations is that a small vertical grid size at the lowest level in a domain containing steeply-sloped topography requires high horizontal resolution for computational stability. From numerical analysis, a guideline here is that the terrain height difference between adjacent grid cells should ideally be less than the vertical grid size. Accordingly, the uniform horizontal grid sizes are chosen to be 0.05, 0.034 and 0.02 m in the simulations with Hills 8, 5 and 3, respectively.

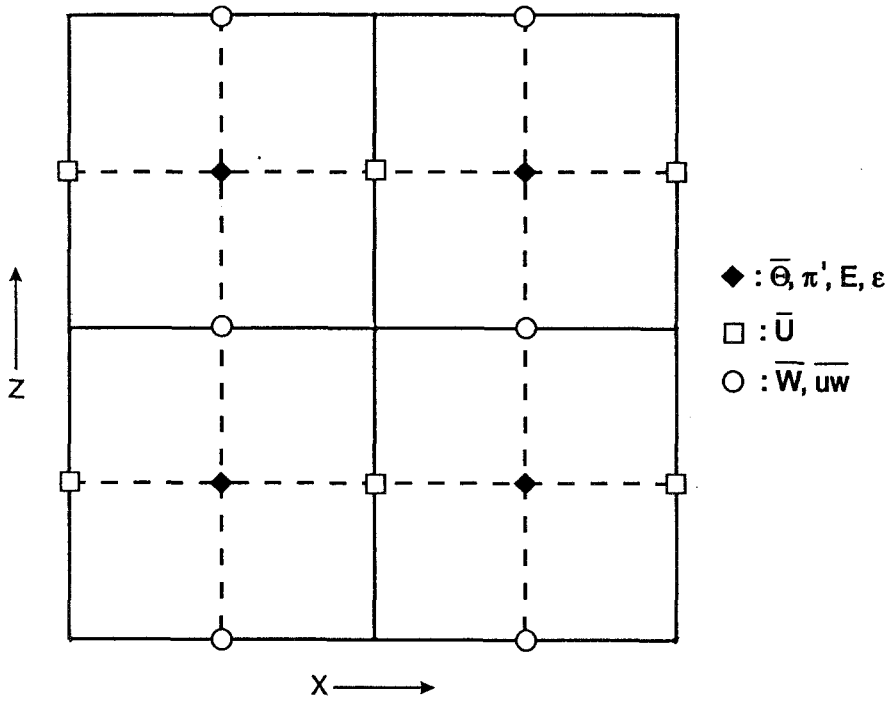

Fig. 1. Schematic picture of the model grid.

5.2. Terrain specification

The shape of the hills installed in the EPA wind tunnel experiment RUSHIL is given by the following parametric equations (Khurshudyan *et al.*, 1981)

$$x = \frac{1}{2}\xi\left[1 + \frac{a^2}{\xi^2 + m^2(a^2 - \xi^2)}\right], \qquad |x| \leq a$$

$$z = \frac{1}{2}m\sqrt{a^2 - \xi^2}\left[1 - \frac{a^2}{\xi^2 + m^2(a^2 - \xi^2)}\right], \tag{29}$$

where

$$m = \frac{h}{a} + \sqrt{\left(\frac{h}{a}\right)^2 + 1},$$

h is the height of the hill, a is the half width of the hill and ξ is an arbitrary parameter.

The hills described by Equation (29) have forms that are symmetric about the z-axis and smoothly merge into a flat plane at the points $x = \pm a$. When the

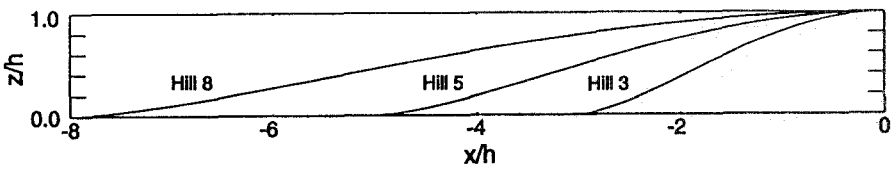

Fig. 2. Shapes of the model hills (to scale) in the EPA experiment RUSHIL.

aspect ratio a/h equals 8, 5 and 3, Equation (29) gives the shape of Hills 8, 5 and 3, respectively, as shown in Figure 2. The surface height $z_g(x)$ in Equation (6) (in the two-dimensional case) needed to define the terrain-following coordinate transformation is obtained from Equation (29) by a numerical scheme of finding roots of a nonlinear algebraic equation.

5.3. Finite-difference scheme

The equations of motion are compressible and thus permit the propagation of sound wave modes. The presence of sound waves can place severe restrictions on the time step in the numerical integration because of their high propagation speed. In order to make such a model economically feasible, a time-splitting integration method (Klemp and Wilhelmson, 1978) is employed in conjunction with a leapfrog time-differencing scheme on the long time step and a forward-backward scheme on the small time step. To remove any tendencies of decoupling odd and even time steps in the leapfrog scheme, an Asselin time smoother (Asselin, 1972) is incorporated in the model. A second-order flux conservative form of advective schemes (Tremback *et al.*, 1987) and second-order centered space differencing to all other derivatives are used in the integration of the prognostic equations.

For computational stability of the model, it is necessary that the time step be set close to, but below the limiting value determined by the Courant-Friedrichs-Lewy (CFL) condition and other factors such as the maximum terrain slope. Through numerical experiments, the long time steps for the simulations of the Hills 8, 5 and 3 cases are determined to be 0.005, 0.002, and 0.00025 s, respectively. In each case, the short time steps are taken to be 5 times smaller than the long time steps.

To attain steady-state values of the computed mean velocity components and turbulence quantities, the simulation must be run for at least 2 s of simulation time (or 40,000 short time steps in the time-splitting integration scheme) in the Hill 3 case. On an IBM RISC/6000-560 workstation, the simulation requires about 80 minutes of CPU time. The Hills 5 and 8 cases require 20 minutes and 6 minutes of CPU time, respectively. Simulations using different turbulence models require about the same amount of CPU time.

6. Results of the Simulations

The vertical profiles of the horizontal wind component $\overline{U}(z)$, the vertical wind component $\overline{W}(z)$ and the Reynolds stress $\overline{uw}(z)$ computed for Hills 8, 5 and 3 by using three different turbulence models (i.e., the standard $E-\epsilon$ model, the ARSM and the $E-\epsilon-\overline{uw}$ model) are compared with all available experimental profiles at 16 longitudinal locations. Figures 3–11 show these profiles at three representative longitudinal locations: $x=-a/2$ (upstream), $x=0$ (hill top) and $x=a$ (downstream). In the following, the results for $\overline{U}(z)$, $\overline{W}(z)$ and $\overline{uw}(z)$ will be discussed separately.

6.1. Results for the horizontal wind component $\overline{U}(z)$

In Figures 3, 6 and 9 the vertical profiles of the horizontal wind component $\overline{U}(z)$ obtained from the simulations with Hills 8, 5 and 3, respectively, are compared with the corresponding measurements. In general, the simulation results agree well with the measurements. Also, the simulation results seem insensitive to the turbulence closure scheme, in agreement with the general assessment by previous studies. Here, the most distinctive feature of the flow pattern is shown on the lee side of Hill 3, where flow separation occurs with the mean flow reversed in the recirculation zone. The presence of this stationary separation zone poses the most difficult and challenging part in the numerical simulations. For example, it is known that the linear theory can not be used to deal with the recirculating flows, and the mixing-length hypothesis is not suitable for this situation either. In Figure 9c, the measured profile $\overline{U}(z)$ in the lee of Hill 3 is characterized by negative values near the ground. As shown in the same figure, the simulation results for $\overline{U}(z)$ obtained by using three different closure models are able to reproduce this reversed flow feature. Specifically, the results obtained using the $E-\epsilon-\overline{uw}$ model are quite satisfactory.

6.2. Results for the vertical wind component $\overline{W}(z)$

In Figures 4, 7 and 10, the vertical profiles of the vertical velocity component $\overline{W}(z)$ obtained from the simulations with Hills 8, 5 and 3, respectively, are compared with the corresponding measurements. The simulation results generally agree well with the measurements. Nevertheless, near the top of the model domain at the lee side locations of Hills 8 and 5 (see Figures 4b and 7b), the simulation results do not quite agree with the measurements. In the simulations, the vertical velocity component $\overline{W}(z)$ naturally approaches zero at the height of 1 m without arbitrary constraints because the rigid lid upper boundary condition is enforced at the 2 m height. This trend seems physically reasonable, considering that at the 1 m height, the flow should reach the freestream limit as shown by the horizontal velocity profiles $\overline{U}(z)$. The experimental results, on the other hand, give non-zero values for $\overline{W}(z)$ at the 1 m height on the lee sides of Hills 8 and 5. We are uncertain about the reason for the disagreement between the simulations and the

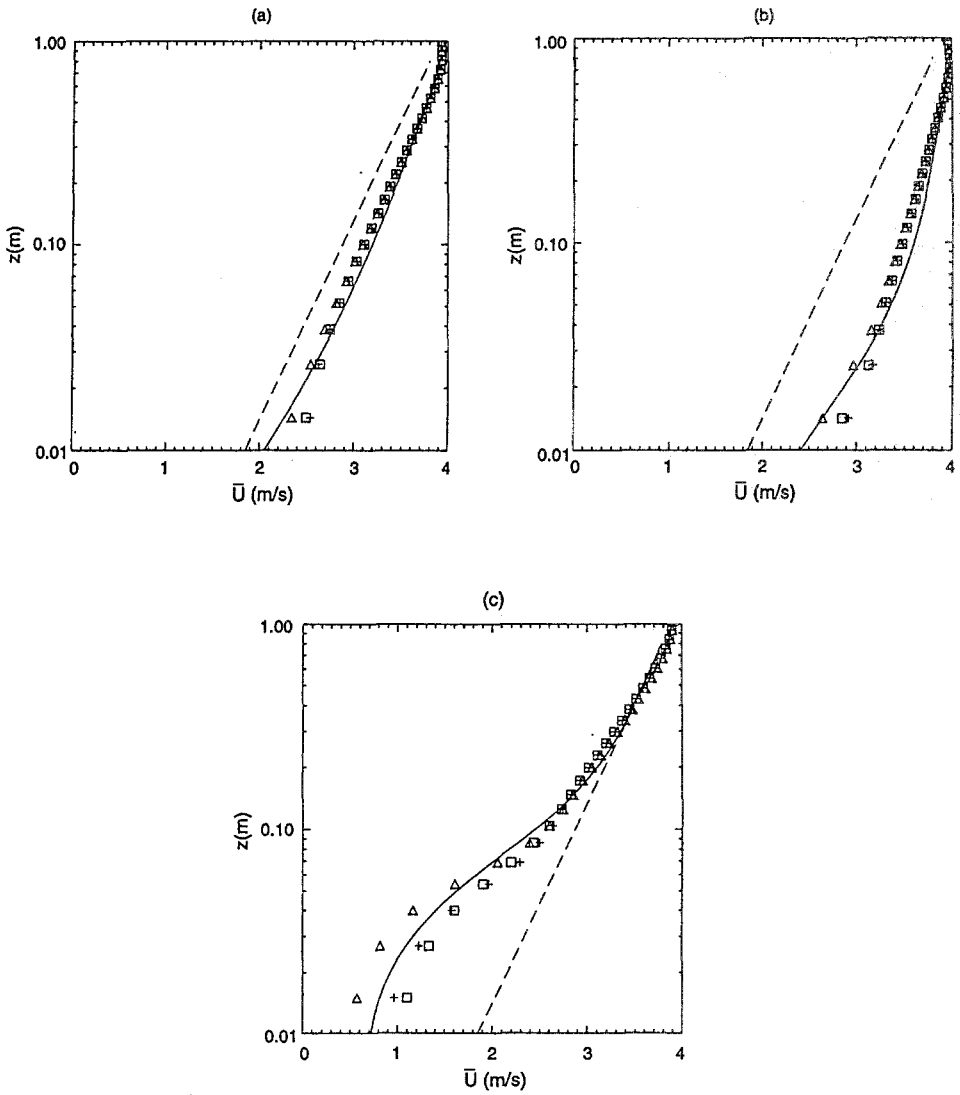

Fig. 3. The vertical profiles of the horizontal mean velocity component $\overline{U}(z)$ over Hill 8 at three longitudinal locations: (a) $x = -a/2$, (b) $x = 0$, (c) $x = a$. The solid line is from the experimental data for Hill 8; the dashed line is from the experimental data for flat terrain; the squares are the simulation results with the standard $E - \epsilon$ model; the triangles are the simulation results with the ARSM; the plus signs are the simulation results with the $E - \epsilon - \overline{uw}$ model.

measurements. We can only speculate that some unknown factor is present in the wind tunnel experiments which is not predicted in the current theoretical model.

Another disagreement in the case of $\overline{W}(z)$ is found near the ground at the top of Hill 3, as shown in Figure 10b. Here, rather large positive values of $\overline{W}(z)$ are measured, from which a large positive value for $\overline{W}$ at ground level

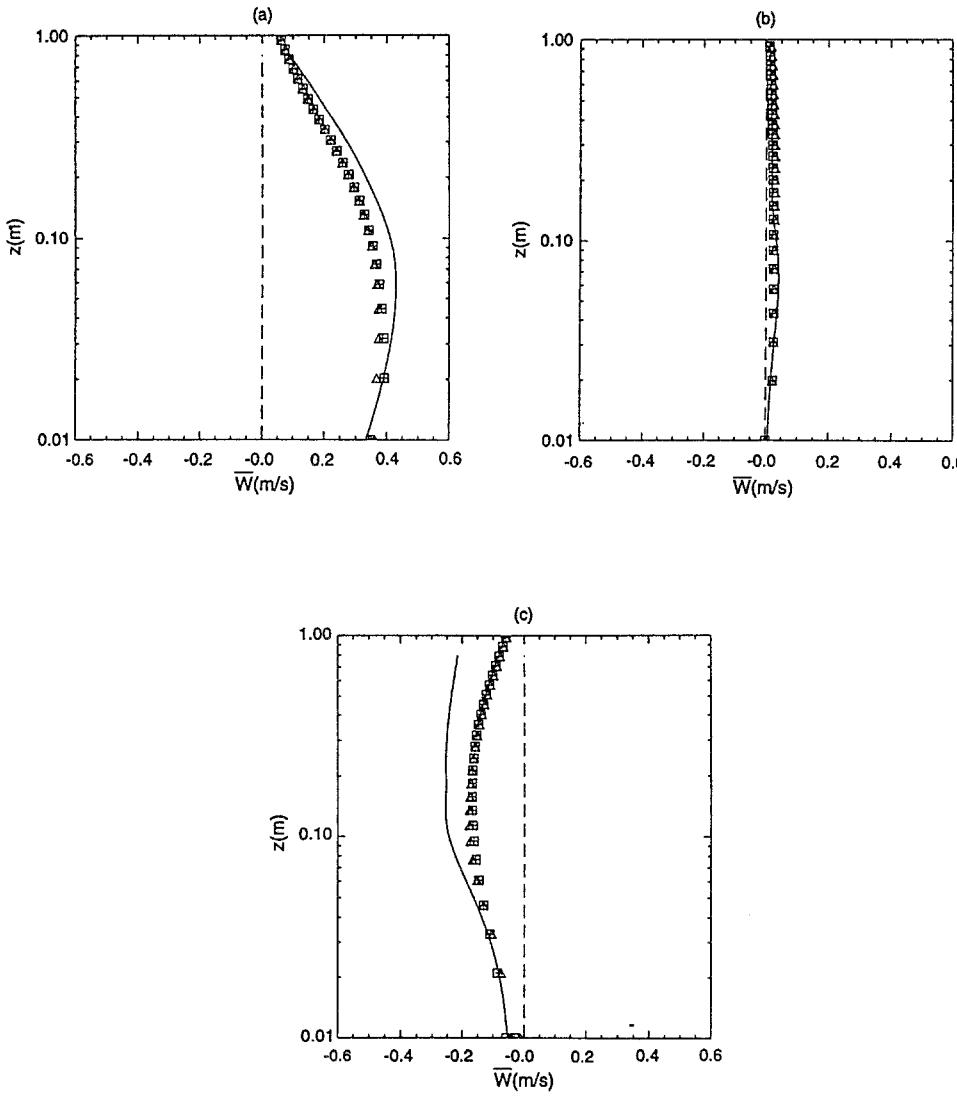

Fig. 4. The same as Figure 3 but for the vertical mean velocity component $\overline{W}(z)$.

is inferred. The simulation, on the other hand, predicts smaller positive values for $\overline{W}(z)$ near the ground and a zero value for $\overline{W}$ at the surface. Large vertical velocities were also measured near the ground on the top of Black Mountain in a field experiment reported by Bradley (1980). In the presence of a prevailing NW wind, Black Mountain can be regarded as a two-dimensional hill with an aspect ratio similar to Hill 3. Bradley described the measured large vertical velocities as "somewhat surprising" but thought that they could possibly be explained in terms of the large-scale separation effects on the lee side. Regarding the same

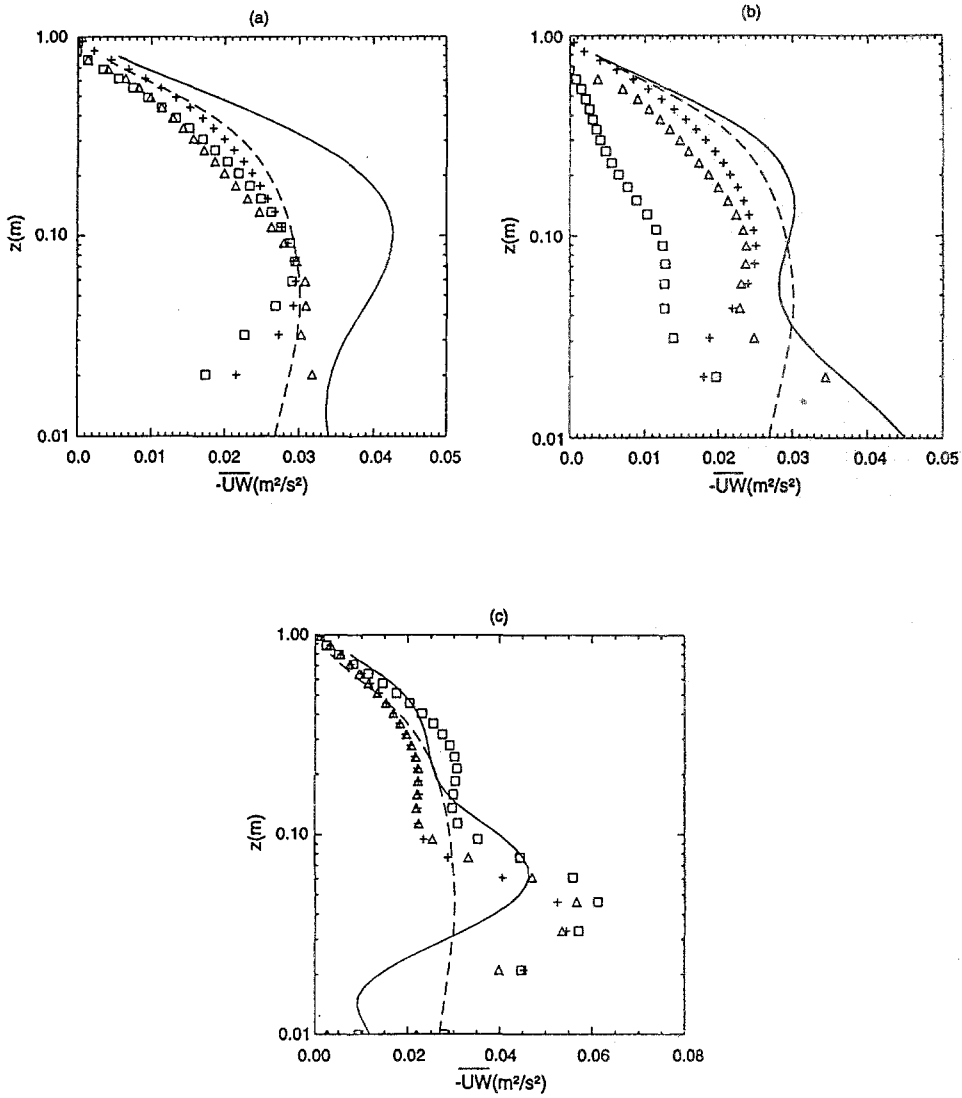

Fig. 5. The same as Figure 3 but for the Reynolds stress $\overline{uw}(z)$.

phenomenon, Zeman and Jensen (1987) speculated that the large slope of the hill probably caused flow separation fairly near the summit. At any rate, our simulation fails to reproduce these large vertical velocities. Evidently, a deeper understanding of the physical processes that affect the vertical velocity is still required. The real question about the measurements, however, is the unphysical, large positive value of $\overline{W}$ at ground level, because at the very top of a hill, the direction of the velocity at the ground should be horizontal in accordance with the surface contour. Possible sources of errors in the experimental data are the

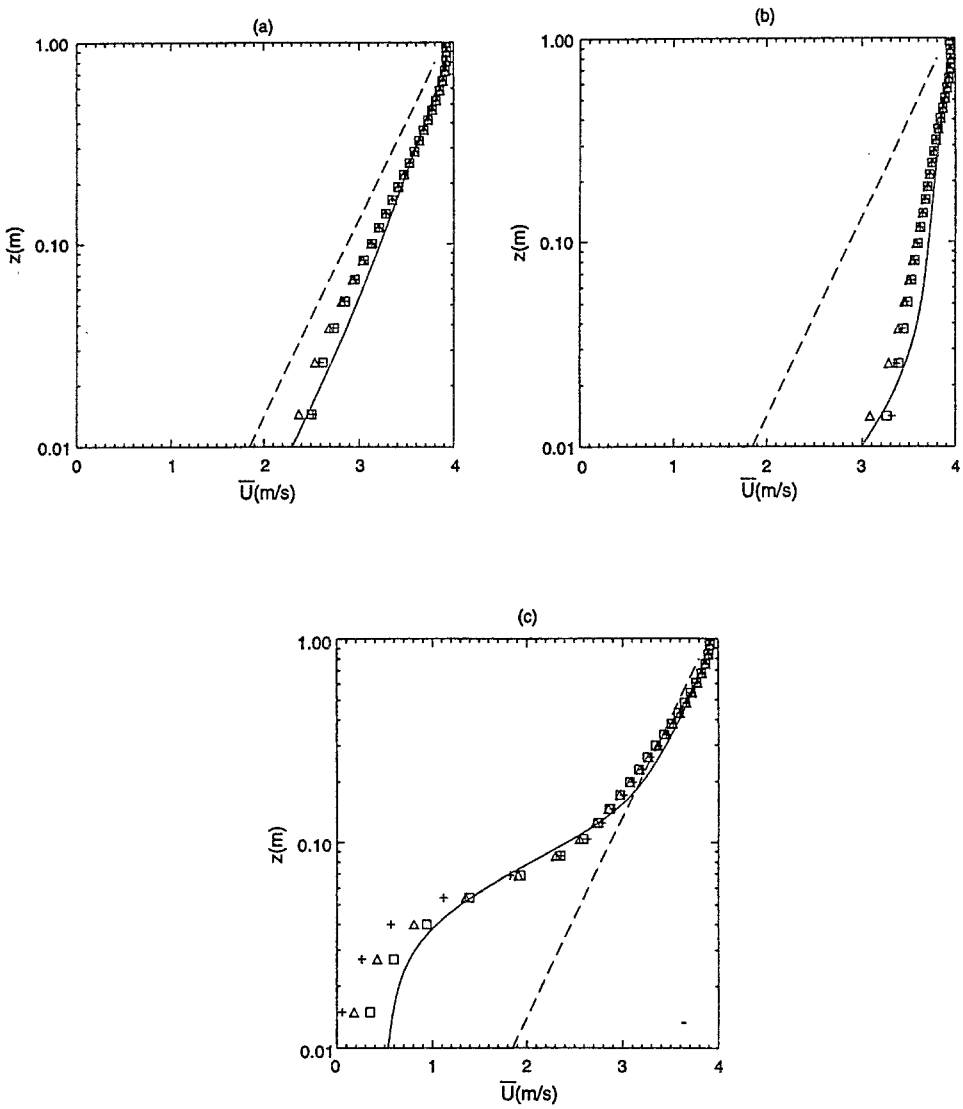

Fig. 6. The vertical profiles of the horizontal mean velocity component $\overline{U}(z)$ over Hill 5 at three longitudinal locations: (a) $x = -a/2$, (b) $x = 0$, (c) $x = a$. The solid line is from the experimental data for Hill 5; the dashed line is from the experimental data for flat terrain; the squares are the simulation results with the standard $E - \epsilon$ model; the triangles are the simulation results with the ARSM; the plus signs are the simulation results with the $E - \epsilon - \overline{uw}$ model.

extreme difficulty of obtaining reliable measurements in the region very close to the ground in a wind tunnel or some flaws in the data smoothing process.

Finardi *et al.* (1993) have recently used two mass-consistent models to simulate the profiles of the mean velocity components $\overline{U}(z)$ and $\overline{W}(z)$ in the EPA wind tunnel experiments RUSHIL. Comparison of their results with ours shows that

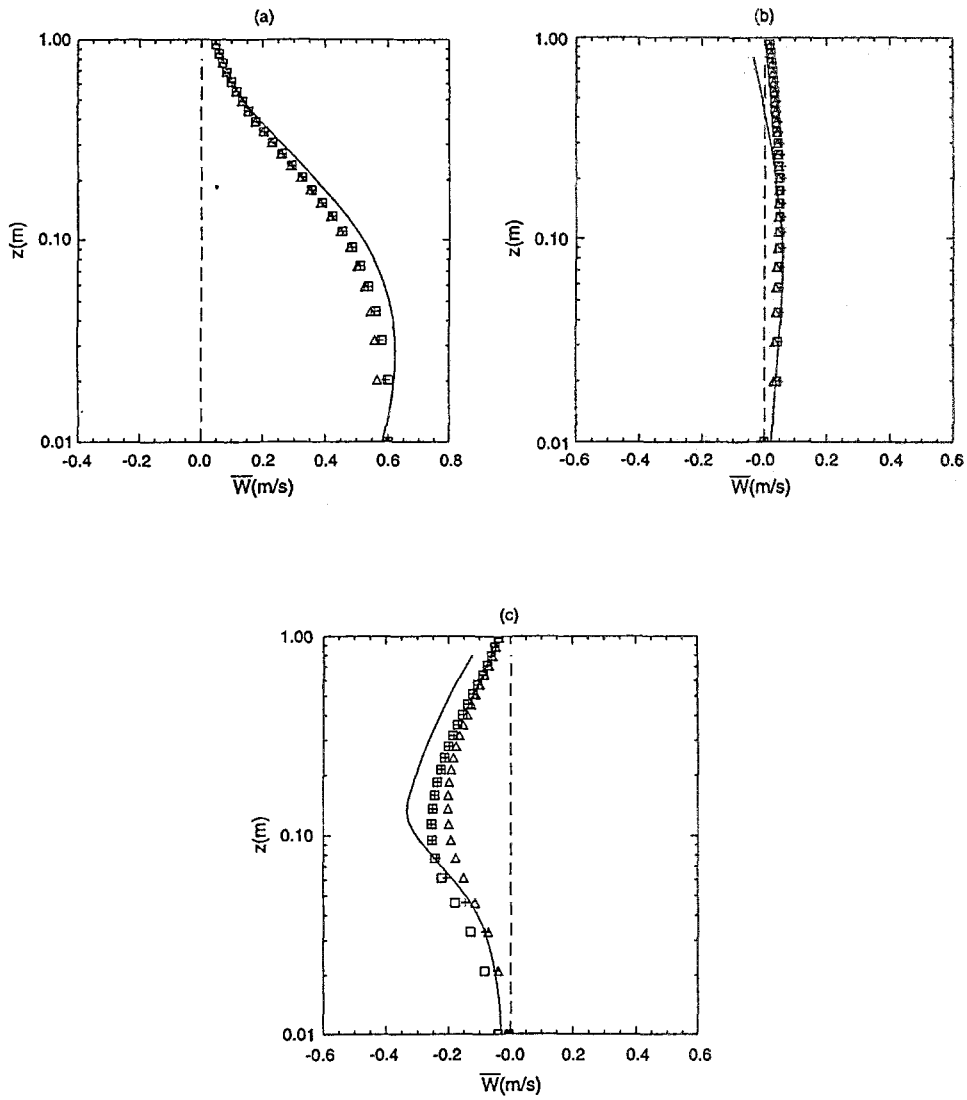

Fig. 7. The same as Figure 6 but for the vertical mean velocity component $\overline{W}(z)$.

the latter generally exhibit better agreement with experiments. Another advantage of our simulations over the mass-consistent models is that the latter require three or four input vertical profiles at different x locations from measurements whereas our simulation does not require any input profiles from measurements except the output equilibrium profiles from the simulation with flat terrain. Furthermore, our model can also incorporate higher-order turbulence closure schemes, which can not be achieved with either linearized or mass-consistent models.

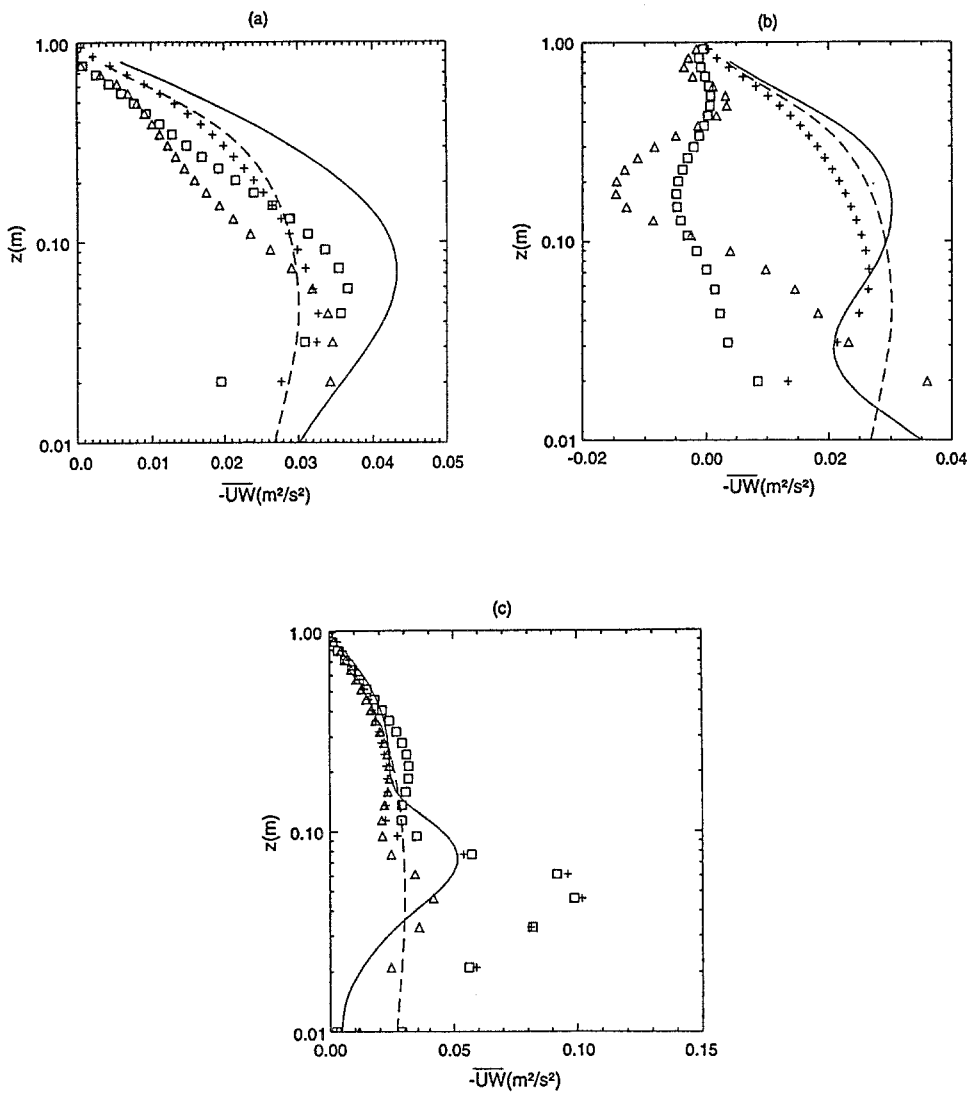

Fig. 8. The same as Figure 6 but for the Reynolds stress $\overline{uw}(z)$.

6.3. Results for the Reynolds stress $\overline{uw}(z)$

In Figures 5, 8 and 11, we compare the model results for the vertical profiles of the Reynolds stress $\overline{uw}(z)$ obtained for Hills 8, 5 and 3 with the corresponding measurements. In general, the simulation results for $\overline{uw}(z)$ do not agree with the measurements as well as in the case for the mean velocity. In addition, the simulated turbulence structure is sensitive to the turbulence closure models used as observed in many other studies (e.g. Taylor *et al.*, 1987; Beljaars *et al.*, 1987).

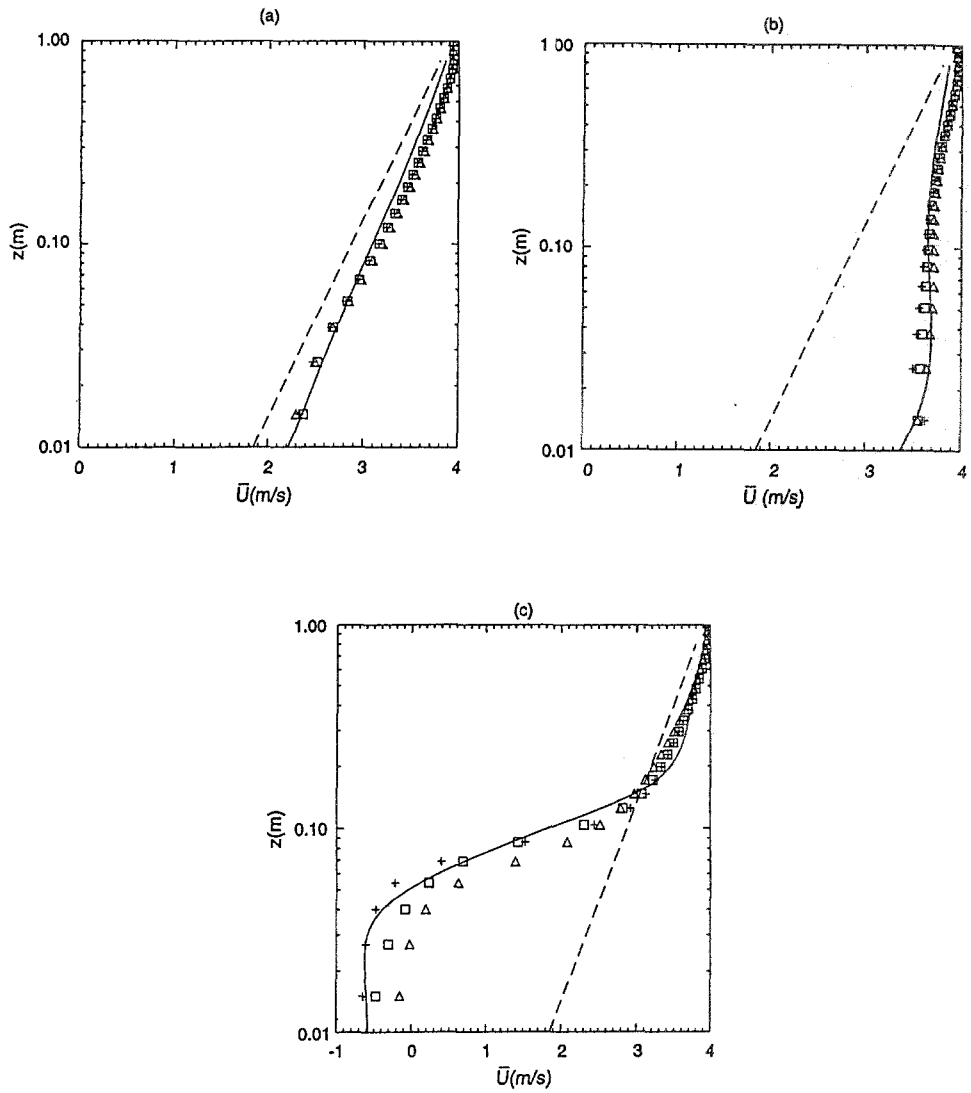

Fig. 9. The vertical profiles of the horizontal mean velocity component $\overline{U}(z)$ over Hill 3 at three longitudinal locations: (a) $x = -a/2$, (b) $x = 0$, (c) $x = a$. The solid line is from the experimental data for Hill 3; the dashed line is from the experimental data for flat terrain; the squares are the simulation results with the standard $E - \epsilon$ model; the triangles are the simulation results with the ARSM; the plus signs are the simulation results with the $E - \epsilon - \overline{uw}$ model.

First, we discuss the results for $\overline{uw}(z)$ at the hill tops as shown in Figures 5b, 8b and 11b, as only these results can be compared with the results from other model studies. The standard $E-\epsilon$ model fails to reproduce the experimental data in all three cases: it predicts too small values for $-\overline{uw}$ especially in Hills 5 and 3, where it even predicts negative values for $-\overline{uw}$. This type of disagreement

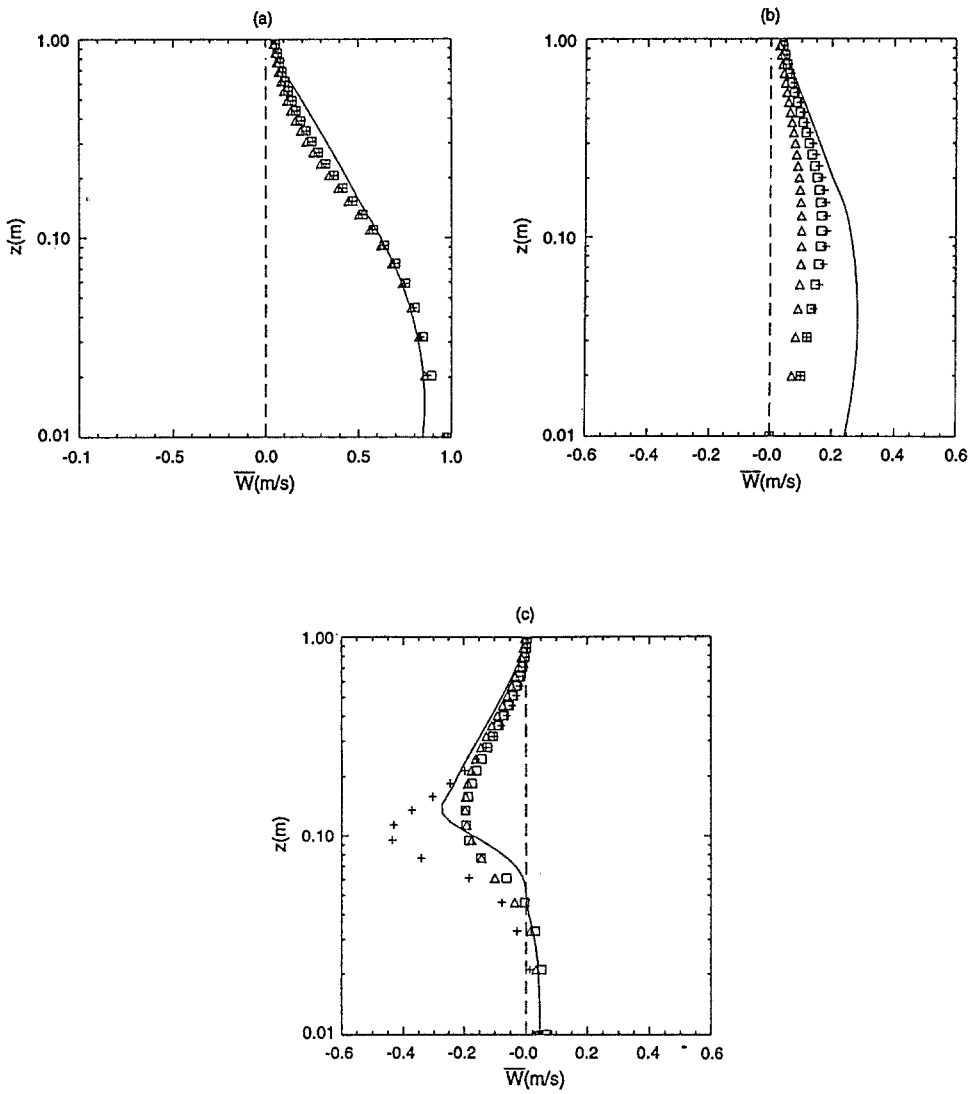

Fig. 10. The same as Figure 9 but for the vertical mean velocity component $\overline{W}(z)$.

was also found in other studies using the $E - \epsilon$ model (Beljaars *et al.*, 1987). As mentioned in the Introduction, the physical reason is that in the outer region within a hilly terrain, the "time of flight" is less than the turbulence decay time, and thus the advection of upstream turbulence can overcome the local lack of production. From the formulation of the $E - \epsilon$ model, however, it is shown that while the advection of E and ϵ is adequately taken into account by the d/dt terms in Equations (10) and (11), it is not so in the case of the Reynolds stresses which are represented only by an eddy-viscosity model, Equation (7). In weak shear

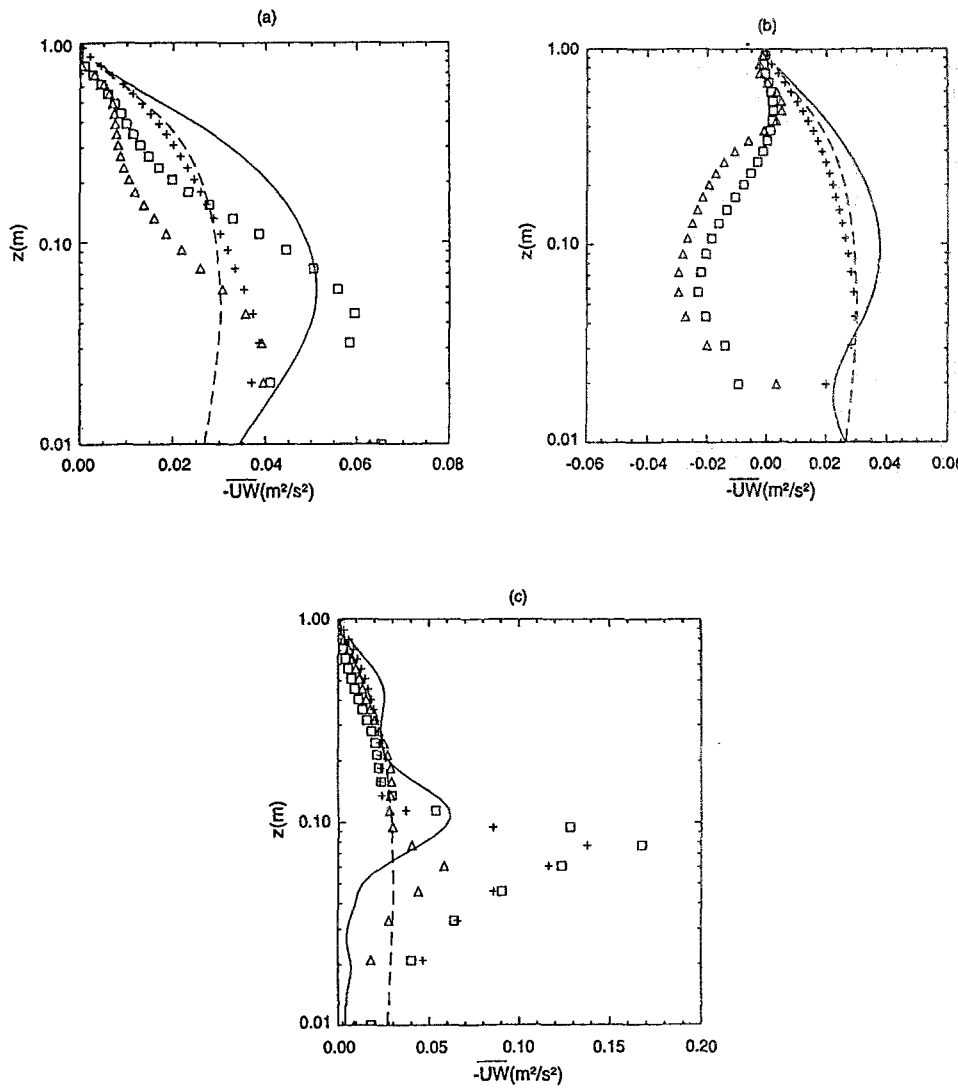

Fig. 11. The same as Figure 9 but for the Reynolds stress $\overline{uw}(z)$.

regions, such as at the hill-top away from the surface, the gradients in Equation (7) become nearly zero or negative, resulting in very small or negative values for $-\overline{uw}$ while the measured $\overline{uw}$ retains more or less its upstream value.

In the Hills 5 and 3 cases, what we observe is a countergradient momentum flux. Originally, the phenomenon of countergradient transport refers to a heat flux when heat is transported from low to high temperature regions (Deardorff, 1966). Analogous to the countergradient heat flux, the turbulent momentum can be transported up and not down the mean velocity gradient as in the Hills 5 and

3 cases. Further theoretical explorations of the countergradient momentum flux can be carried out along the same lines as in the studies on the countergradient heat flux by Deardorff (1972) and Schumann (1987). Here, we only want to indicate that the primary importance of the advection process represented by the d/dt term in the transport Equations (13) for the turbulent momentum fluxes is responsible for a countergradient momentum flux.

The ARSM is only partially successful in predicting the shear stress $\overline{uw}(z)$ at hill tops. Figure 5b shows an improved result for $-\overline{uw}(z)$ at the top of Hill 8. For Hills 5 and 3, however, the simulated results for $\overline{uw}(z)$ shown in Figures 8b and 11b seem to be further away from the measured data than those obtained from the standard $E-\epsilon$ model. The drastically different performances of this type of ARSM with different hills are a clear indication of the limitation of the model. Since Equation (17) retains the form of a down-gradient eddy viscosity model with a positive (though variable) eddy viscosity, it cannot describe countergradient momentum fluxes. Thus, we conclude that this type of ARSM can only apply to low hills where countergradient momentum fluxes are not present.

Considering the complexity of the turbulent processes in flow over a hill, the results for $\overline{uw}(z)$ on hill tops obtained by using the $E-\epsilon-\overline{uw}$ closure model are quite satisfactory. It still appears that the simulations are more successful in the outer layer than in the inner layer, especially in the case of Hill 8. Less satisfactory results for $\overline{uw}$ near the surface at the hill top are also reported in other studies using second-order turbulence closure (Zeman and Jensen, 1987; Beljaars *et al.*, 1987), for which these authors gave inconclusive explanations. We realize that the dominant mechanism in the inner region may not be sufficiently emphasized in such a formulation. Also, the lower boundary conditions used in the simulations are inconsistent with the observation that there is no constant-stress surface layer at the hill top.

As to the results for $\overline{uw}$ at the upstream locations shown in Figures 5a, 8a and 11a, the agreement between the simulations and measurements by all three turbulence models is only marginal. No clear improvement is found in either the ARSM or the $E-\epsilon-\overline{uw}$ model. In general, the understanding of the mechanism that rules the upstream turbulence is still very rudimentary. Very few experimental or theoretical studies were aimed at the upstream turbulence structure. Zeman and Jensen (1987) predicted a shear stress $\overline{u_1 u_3}$, which is defined in the frame of reference aligned with the streamlines, along the windward side of the hill. Their model predictions can be explained solely by the streamline curvature effects; that is, the convex curvature reduces the stress and the concave curvature amplifies the stress. Since we have not included curvature modifications in the $E-\epsilon$ model and the ARSM, and the transport equation for $\overline{uw}$ in our study is written in the Cartesian coordinate system unlike that for $\overline{u_1 u_3}$ in Zeman and Jensen's study (which is written in the streamline coordinate system), we are not able to single out the curvature effects in our study. Some comparison can be made under the assumption that $\overline{uw}$ in our study should behave in a manner similar to that of

$\overline{u_1 u_3}$ in Zeman and Jensen's study. It is shown that the EPA wind tunnel data for $\overline{uw}$ do not quite follow the simple pattern predicted by the curvature effects alone. According to the experimental data, other physical processes must play a role. Again, only better understanding of the dynamical effects on the upstream side of the hill can lead to more successful modeling.

Comparing with the experimental data, the simulation results for $-\overline{uw}$ on the lee side of the hills shown in Figures 5c, 8c and 11c are generally overestimated. The results from the $E-\epsilon-\overline{uw}$ model turn out to be very close to those from the standard $E-\epsilon$ model. The most remarkable feature on the lee side of the hills is a very large mean shear (see Figures 5a, 8a and 11a), the effects of which are two-fold. First, it makes the production term in the transport equation for $\overline{uw}$ so overwhelmingly large that the transport equation for $\overline{uw}$ becomes virtually an eddy viscosity relation like that in the standard $E-\epsilon$ model. Second, in the $E-\epsilon$ and $E-\epsilon-\overline{uw}$ models, because $-\overline{uw}$ is proportional to the mean shear, it yields a very large $-\overline{uw}$.

In the Hills 5 and 3 cases, the results predicted by the ARSM for $\overline{uw}$ are substantially smaller than those predicted by the $E-\epsilon$ and $E-\epsilon-\overline{uw}$ models and seem close to the measured data. This is somewhat unexpected at first, but a closer look at the formulation of the ARSM shows that the variable eddy coefficient decreases with an increased mean shear and thus effectively offsets the large mean shear factor.

On the other hand, measurements of the shear stress on the lee side of a hill are rare and we have not been able to find other measurements to make quantitative comparisons. Teunissen *et al.* (1987) compared the results from wind tunnel simulations of the flow over Askervein hill and the full-scale data from field measurements. They reported that the prototype data appear to display an increase in turbulence intensity in the wake significantly larger than do the wind tunnel measurements. We do not know if there is a similar problem with the EPA wind tunnel measurements. For one thing, the measured turbulence shear stress $\overline{uw}$ to the lee of the hills increased only moderately from its upstream value. We wonder if these measurements are reliable since it is generally believed that the turbulence intensity on the lee side of the hills is very high (cf. Taylor *et al.*, 1987). At this point, we can only conclude that the large discrepancy in the results for the shear stress $\overline{uw}$ to the lee of hills either points to deficiencies in the turbulence models or errors in the measurements.

7. Conclusions and Future Work

Numerical simulations of turbulent flow over two-dimensional hills with different slope have been performed using a finite-difference method in a non-hydrostatic atmospheric model. Computations of the mean and turbulence flows with three different turbulence closure schemes, i.e., the standard $E-\epsilon$ model, the ARSM and the $E-\epsilon-\overline{uw}$ model, have been compared with each other and with

measurements from the EPA wind tunnel experiment RUSHIL. Our findings can be summarized as follows:

1. The simulated mean flow velocities agree well with the measurements. Specifically, the flow separation on the lee side of Hill 3 is well predicted by the simulations. Moreover, the results for the mean velocities are insensitive to the turbulence models used.
2. The simulated results for the turbulent shear stress $\overline{uw}$ depend strongly on the turbulence models used. Generally, the $E-\epsilon-\overline{uw}$ model yields the best agreement with measurements.
3. In predicting the shear stress $\overline{uw}$ on hill tops, the $E-\epsilon-\overline{uw}$ model works well; the standard $E-\epsilon$ model fails and the ARSM is only partially successful. In the outer region, advection of the upstream turbulence dominates and only a transport equation for $\overline{uw}$ can realistically model the advection effects.
4. In predicting the shear stress on the upstream sides and lee sides of hills, there are discrepancies between model predictions and the measurements, which point to deficiencies either in the turbulence models or in the measurements. Further theoretical and experimental studies are needed to ascertain the turbulence dynamics at these locations.

As to the possible directions of improving the model results, the first consideration concerns the constants appearing in the standard $E-\epsilon$ model. The constants used in this study, taken from Launder and Spalding (1972), are based on extensive experimental data in engineering flows. When the $E-\epsilon$ model was applied to the atmosphere, many authors (Detering and Etling, 1985; Raithby *et al.*, 1987; Dawson *et al.*, 1987; Duynkerke, 1988) believed that these constants should be modified. As a result, many different sets of constants have been tried in the atmospheric studies. Among these constants, the most controversial is c_μ, which determines the lower boundary condition for E and should be consistent with the measured value of E, if available. Because of the lack of measurement data for E in the EPA experiment, we can not be sure about the proper value for c_μ, and therefore we did not change it. Hopefully, new experimental evidence will shed light on this matter.

The second consideration concerns the constant coefficients in the transport equation for $\overline{uw}$ (19), which determine the relative weight of each term. These constants are by no means uniquely defined. When the values of these constants change, different physical processes will be emphasized. For example, as stated in the Introduction, the mechanism dominating the turbulence dynamics in the inner layer is different than in the outer layer. It is conceivable that under proper specifications of these constants, the dominating physical process in the inner layer could be sufficiently emphasized to improve the results for $\overline{uw}$ there.

Other directions of research are: (i) to improve the modeling of the pressure-correlation and the third-order moment terms in the transport equations for the second-order moments, (ii) to solve the complete set of transport equations for

the second-order turbulence quantities, and (iii) to use more accurate numerical schemes. These studies are now in progress.

Acknowledgement

R. Ying and R. M. Ypma would like to acknowledge financial support from ENEL-CRTN. Simulations were produced with the Regional Atmospheric Modeling System (RAMS). RAMS was developed at the Colorado State University under the support of the National Science Foundation (NSF) and the Army Research Office (ARO).

References

Asselin, R.: 1972, 'Frequency Filter for Time Integrations', *Mon. Wea. Rev.* **100**, 487–490.

Beljaars, A. C. M., Walmsley, J. L., and Taylor, P. A.: 1987, 'A Mixed Spectral Finite-Difference Model for Neutrally Stratified Boundary-Layer Flow over Roughness Changes and Topography', *Boundary-Layer Meteorol.* **38**, 273–303.

Bradley, E. F.: 1980, 'An Experimental Study of the Profiles of Wind Speed, Shearing Stress and Turbulent Intensities at the Crest of a Large Hill', *Quart. J. Roy. Meteorol. Soc.* **106**, 101–124.

Britter, R. E., Hunt, J. C. R., and Richards, K. J.: 1981, 'Airflow over a Two-Dimensional Hill: Studies of Velocity Speed-Up, Roughness Effects and Turbulence', *Quart. J. Roy. Meteorol. Soc.* **107**, 91–110.

Clark, T. L.: 1977, 'A Small-Scale Dynamic Model Using a Terrain-Following Coordinate Transformation', *J. Computational Phys.* **24**, 186–215.

Dawson, P., Stock, D. E., and Lamb, B.: 1991,'The Numerical Simulation of Airflow and Dispersion in Three-Dimensional Atmospheric Recirculation Zones', *J. Appl. Meteorol.* **30**, 1005–1024.

Deardorff, J. W.: 1966, 'The Counter-Gradient Heat Flux in the Lower Atmosphere and in the Laboratory', *J. Atmos. Sci.* **23**, 503–506.

Deardorff, J. W.: 1972, 'Theoretical Expression for the Countergradient Vertical Heat Flux', *J. Geophys. Res.* **77**, 5900–5904.

Detering, H. W. and Etling, D.: 1985, 'Application of the $E - \epsilon$ Turbulence Model to the Atmospheric Boundary Layer', *Boundary- Layer Meteorol.* **33**, 113–133.

Duynkerke, P. G.: 1988, 'Application of the $E - \epsilon$ Turbulence Closure Model to the Neutral and Stable Atmospheric Boundary Layer', *J. Atmos. Sci.* **45**, 865–880.

Finardi, S., Brusasca, G., Morselli, M. G., Trombetti, F., and Tampieri, F.: 1993, 'Boundary-Layer Flow over Analytical Two-Dimensional Hills: A Systematic Comparison of Different Models with Wind Tunnel Data', *Boundary-Layer Meteorol.* **63**, 259–291.

Hanjalic, K. and Launder, B. E.: 1972, 'A Reynolds Stress Model of Turbulence and Its Application to Thin Shear Flows', *J. Fluid Mech.* **52**, 609–638.

Hunt, J. C. R. and Simpson, J. E.: 1982, 'Atmospheric Boundary Layer over Non-Homogeneous Terrain', in E. J. Plate (ed.), *Engineering Meteorology*, Elsevier, Amsterdam.

Khurshudyan, L. H., Snyder, W. H., and Nekrasov, I. V.: 1981, 'Flow and Dispersion of Pollutants over Two-Dimensional Hills'. U.S. Envir. Prot. Agcy. Rpt. No. EPA-6000/4-81-067. Res. Tri. Pk., NC., 131 pp.

Klemp, J. B. and Wilhelmson, R. B.: 1978, 'The Simulation of Three-Dimensional Convective Storm Dynamics', *J. Atmos. Sci.* **35**, 1070–1096.

Lang, N. J. and Shih, T. H.: 'A Critical Comparison of Two-Equation Turbulence Models', NASA Technical Mem. 105237.

Launder, B. E. and Spalding, D. B.: 1974, 'The Numerical Computations of Turbulent Flows', *Comp. Mech. in Appl. Mech. and Eng.* **3**, 269–289.

Mason, P. J. and King, J. C.: 1985, 'Measurements and Predictions of Flow and Turbulence over an Isolated Hill of Moderate Slope', *Quart. J. Roy. Meteorol. Soc.* **111**, 617–640.

Pielke, R. A.: 1984, 'Mesoscale Meteorological Modeling', Academic Press, New York, 612 pp.
Raithby, G. D., Stubley, G. D., and Taylor, P. A.: 1987, 'The Askervein Hill Project: A Finite Control Volume Prediction of Three-Dimensional Flows over the Hill', *Boundary-Layer Meteorol.* **39**, 247–267.
Rodi, W.: 1984, 'Turbulence Models and Their Application in Hydraulics', IAHR, Netherlands.
Schumann, U.: 1987, 'The Countergradient Heat Flux in Turbulent Stratified Flows', *Nucl. Eng. Design* **100**, 255–262.
Taylor, P. A., Mason, P. J., and Bradley, E. F.: 1987, 'Boundary-Layer Flow over Low Hills', *Boundary-Layer Meteorol.* **39**, 107–132.
Teunissen, H. W., Shokr, M. E., Bowen, A. J., Wood, C. J., and Green, D. W. R.: 1987, 'The Askervein Hill Project: Wind-Tunnel Simulations at Three Length Scales', *Boundary-Layer Meteorol.* **40**, 1–29.
Tremback, C. J., Powell, J., Cotton, W. R., and Pielke, R. A.: 1987, 'The Forward-in-Time Upstream Advection Scheme: Extension to Higher Orders', *Mon. Wea. Rev.* **115**, 540–555.
Trombetti, F., Martano, P., and Tampieri, F.: 1991, 'Data Sets for Studies of Flow and Dispersion in Complex Terrain: I) The "RUSHIL" Wind Tunnel Experiment (Flow Data)', Technical Report No.4, FISBAT-RT-91/1.
Zeman, O. and Jensen, N. O.: 1987, 'Modification of Turbulence Characteristic in Flow over Hills', *Quart. J. Roy. Meteorol. Soc.* **113**, 55–80.